Angstrom-scale spectroscopic visualization of interfacial interactions in an organic/borophene vertical heterostructure

Linfei Li[a], Jeremy F. Schultz[a], Sayantan Mahapatra[a], Xiaolong Liu[b#], Chasen Shaw[c], Xu Zhang[c], Mark C. Hersam[b,d,e,f], and Nan Jiang[a]*

[a]Department of Chemistry, University of Illinois at Chicago, Chicago, Illinois 60607, United States.

[b]Applied Physics Graduate Program, Northwestern University, Evanston, Illinois 60208, United States.

[c]Department of Physics and Astronomy, California State University, Northridge, Northridge, California 91330, United States.

[d]Department of Materials Science and Engineering, Northwestern University, Evanston, Illinois 60208, United States.

[e]Department of Chemistry, Northwestern University, Evanston, Illinois 60208, United States.

[f]Department of Electrical and Computer Engineering, Northwestern University, Evanston, Illinois 60208, United States.

*Email: njiang@uic.edu

Abstract

Two-dimensional boron monolayers (i.e., borophene) hold promise for a variety of energy, catalytic, and nanoelectronic device technologies due to the unique nature of boron-boron bonds. To realize its full potential, borophene needs to be seamlessly interfaced with other materials, thus motivating atomic-scale characterization of borophene-based heterostructures. Here, we report the vertical integration of borophene with tetraphenyldibenzoperiflanthene (DBP) and measure their angstrom-scale interfacial interactions with ultra-high vacuum tip-enhanced Raman spectroscopy (TERS). In addition to identifying the vibrational signatures of adsorbed DBP, TERS reveals subtle ripples and compressive strains of the borophene lattice underneath the molecular layer. The induced interfacial strain is demonstrated to extend in borophene by ~1 nm beyond the molecular region by virtue of 5 Å chemical spatial resolution. Molecular manipulation experiments prove the molecular origins of interfacial strain in addition to allowing atomic control of local strain with magnitudes as small as ~0.6%. Besides being the first realization of an organic/borophene vertical heterostructure, this study demonstrates UHV-TERS is a powerful analytical tool to spectroscopically investigate buried and highly localized interfacial characteristics at the atomic scale, which can be applied to additional classes of heterostructured materials.

Introduction

Experimentally realized two-dimensional (2D) boron sheets (that is, borophene) have attracted immense attention as a promising 2D platform with multiple physical and chemical features that could be tuned for investigations of fundamental science and device applications.[1,2] Borophene possesses unique structural characteristics and superlative physical properties, such as polymorphism, in-plane anisotropy, superconductivity, and existence of Dirac fermions[3-12]. As the lightest and thinnest 2D material, of particular interest are its remarkable chemical and mechanical properties, including extremely high bending flexibility and in-plane elasticity that arise from the unique nature of boron-boron bonds.[13,14] These exceptional qualities allow ultrasensitive mechanical responses to local interactions, and promise considerable structural compliance that can enable seamless interfaces with disparate materials for various practical applications.[10,11,15] Despite this potential, the integration of borophene into heterostructures is still at a nascent stage.[16,17] Drawing inspiration from other 2D materials, organic functionalization enables diverse heterostructures by providing tailored chemical reactivity or passivating buffer layers.[18-24] To this end, early efforts were made to functionalize borophene with perylenetetracarboxylic dianhydride (PTCDA) molecules. However, the higher adsorption enthalpy of PTCDA on the Ag(111) substrate rather than borophene resulted in the formation of a structurally and electronically abrupt borophene-organic lateral heterostructure.[16] Consequently, to date, organic decoration of borophene and resulting functionalized heterostructures have not been realized experimentally despite their promise for modifying borophene chemistry and interfacial properties.

Interfacial structures and interactions play a significant role in determining the fundamental properties and essential functionalities of heterostructured materials.[25-28] For example, interfacial strains formed in lateral and vertical heterostructures have provided band-engineering strategies to tailor their electronic and vibrational properties, facilitating (opto-)electronic applications.[29-32] Given their potential for heterogeneity and variation at the nanoscale, the chemically resolved interrogation of interfacial features at the atomic level is necessary to reveal the local nature of heterostructural properties. Towards this end, scanning tunneling microscopy and spectroscopy (STM/STS) have allowed structural and electronic characterizations of borophene-based lateral heterostructures with angstrom precision, but have provided limited chemical information and minimal insight into the nature of interfacial interactions.[16,17] While *in situ* X-ray photoelectron spectroscopy has shed light on the noncovalent nature of lateral organic-borophene bonding,[16] the ensemble averaging of this technique lacks spatial resolution and thus cannot identify site-resolved phenomena. In contrast, tip-enhanced Raman spectroscopy (TERS), an optical near-field technique, integrates the chemical specificity of plasmon-enhanced Raman spectroscopy with the spatial resolution of a scanning probe microscope.[33-40] It can therefore provide chemical signature and topographic information simultaneously. Notably, when performed under ultra-high vacuum (UHV) conditions, TERS allows the elucidation of chemical details down to the sub-nanoscale regime.[41-53] These exceptional capabilities suggest that UHV-TERS is an ideal characterization tool for highly localized structural and chemical properties of low-dimensional materials and their heterostructures including strain, defects, and doping.[54,55] In particular, interfacial characteristics that determine properties are physically buried in vertical heterostructures, making them inaccessible via common

surface imaging methods; such a challenge could be overcome by acquiring spatially resolved vibrational spectroscopy and subsequent subsurface imaging via TERS.

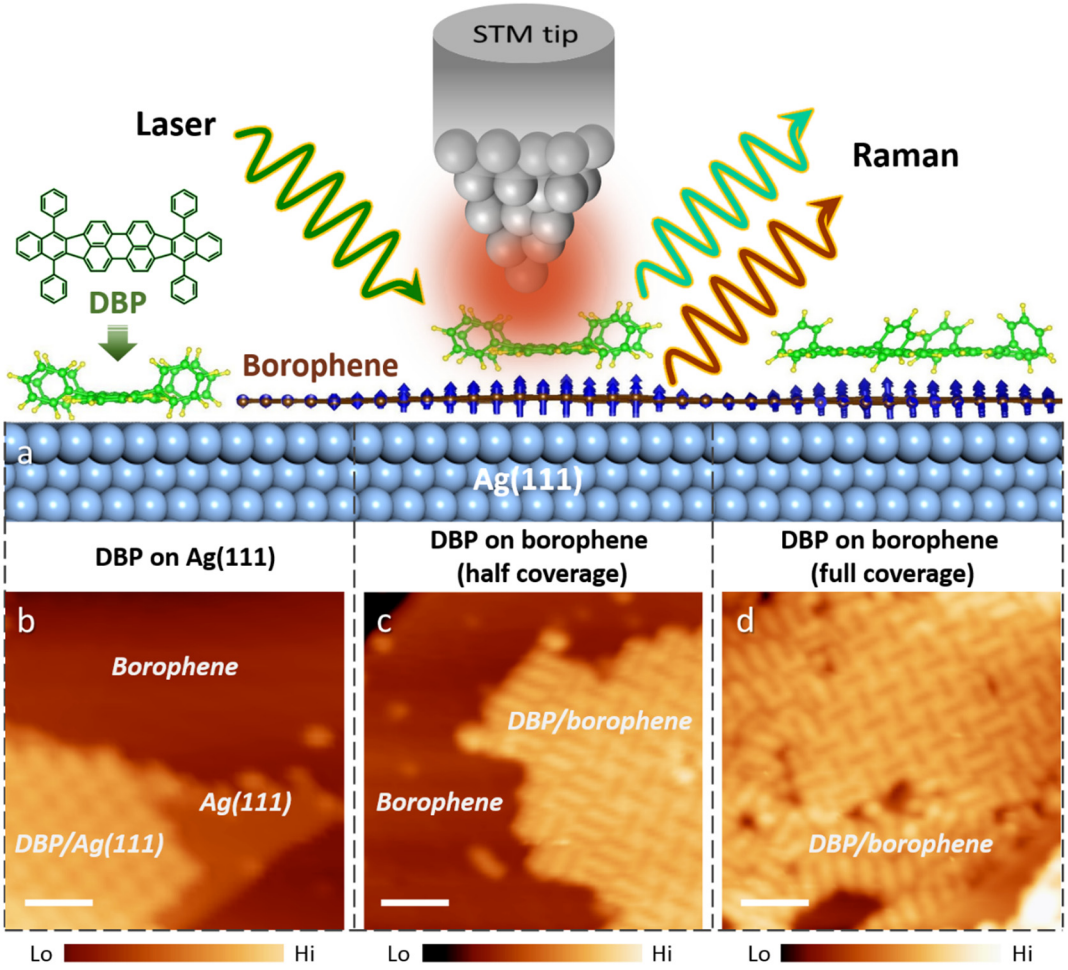

Figure 1. Combined UHV-STM and UHV-TERS studies of DBP/borophene vertical heterostructures. (a) Experimental schematic including the molecular structure of DBP. The blue arrows denote boron atomic displacements in the borophene monolayer. (b-d) STM topographs show the results of depositions of DBP molecules on sub-monolayer borophene on Ag(111) with increasing coverage [(b) 1.5 V, 300 pA; (c) 1.5 V, 50 pA; (d) 1.5 V, 200 pA. Scale bars: 4 nm]. The corresponding derivative STM images, which show the borophene structures more clearly, are presented in Figure S2.

Here, we report the first experimental realization of an organic/borophene vertical heterostructure with tetraphenyldibenzoperiflanthene (DBP), and present studies of their angstrom-scale interfacial interactions via combined UHV-STM, UHV-TERS, and density functional theory (DFT) (Figure 1a). The chosen DBP molecule has been an archetypical system for understanding molecular self-assembly on metal surfaces,[56,57] and is widely used as an organic electron donor in photovoltaic cells and as a fluorescent emitter dopant in light-emitting devices.[58,59] Fine control over molecular deposition on sub-monolayer borophene results in the formation of DBP/borophene vertical heterostructures, as exemplified in Figure 1c,d. In addition to identifying the vibrational fingerprints of

adsorbed DBP on borophene, TERS measurements extend their conformational and chemical sensitivity to the underlying vertical interfaces that are inaccessible solely via STM, thereby spectroscopically visualizing gentle undulations and in-plane compression of the borophene lattice under the molecules. In particular, by taking advantage of ~5 Å chemical spatial resolution of UHV-TERS, extremely localized interfacial strain in borophene is probed as a result of a delicate "strain spillover" effect. The molecular origin of the induced strain is verified by showing that the strain can be released in a reversible fashion through the removal of adsorbed molecules via STM-controlled molecular manipulation. The ability to induce and control local strain in borophene suggests a generalizable approach for strain engineering of 2D materials via organic modification, which could enable strain-coupled properties to be tuned and tailored in the angstrom-scale regime.

Results and Discussion

Growth and characterizations of borophene

The fabrication of DBP/borophene heterostructures begins with borophene. Borophene is produced by bottom-up synthesis in UHV via physical vapor deposition of boron atoms onto metal substrates,[1,2,60-62] such as the Ag(111) surface used in the present study (Figure 2a). Unlike graphene that solely adopts a honeycomb-like lattice, borophene possesses rich structural diversity (i.e., polymorphism), which was predicted theoretically[5,6] and then realized on Ag(111)[1-4] (Figure 2a). Borophene polymorphs are characterized by a network of vacancies (i.e., hollow hexagons) within a triangular lattice with diverse periodic distributions.[5,6,11] Depending on the growth temperature, two prominent structural polymorphs of borophene have been synthesized on Ag(111) – i.e., $\nu_{1/6}$ and $\nu_{1/5}$ (fractions denote the concentration of vacancies in an otherwise triangular lattice), as shown in Figure 2b-d. The polymorphic nature of borophene underlies its promising chemical and mechanical properties. In particular, the diversity of boron-boron bonding geometries suggests rich possibilities when chemically modifying borophene, which can facilitate the integration of borophene into 2D heterostructures.

The structural properties of borophene were further examined with TERS at 78 K using a 561 nm laser (8 mW). Consistent with a previous TERS characterization of pristine borophene,[63] the spectra acquired above the $\nu_{1/6}$ (red) and $\nu_{1/5}$ (blue) phases show characteristic 189 cm^{-1} and 180 cm^{-1} peaks, respectively (Figure 2e), which are assigned to the B_{3g}^2 ($\nu_{1/6}$) and B_g^2 ($\nu_{1/5}$) Raman modes, with the other vibrational modes significantly less enhanced. The pronounced enhancement of the B_{3g}^2 ($\nu_{1/6}$) and B_g^2 ($\nu_{1/5}$) modes, whose vibrational motions are both perpendicular to the borophene plane (as discussed later in Figure 4e,f), is attributed to the surface selection rules of TERS.[64] Specifically, in TERS the most enhanced vibrational modes contain components parallel to the axial plasmonic field under the tip (i.e., perpendicular to the surface; z-component). In turn, the selection rules imply that these vibrational modes should be sensitive to out-of-plane perturbations, such as molecular adsorption or heterolayer stacking.

Beyond point spectra, the local structural distribution of borophene can be readily identified via TERS line scans and 2D mapping. Figure 2f plots the line spectra (14 consecutive TERS measurements), which were acquired along the green-line trace in the inset of Figure 2e. Notably, the Raman spectra at positions 1-7 feature the 189 cm^{-1} peak

of the $v_{1/6}$ phase shown in Figure 2e, while those at positions 8-14 feature the 180 cm^{-1} peak of the $v_{1/5}$ phase. The line profiles extracted from these spectra, exhibiting the intensity evolution of the 189 cm^{-1} and 180 cm^{-1} peaks, provide clear fingerprint identification of the $v_{1/6}$ and $v_{1/5}$ phases with a spatial resolution of 5 Å. Furthermore, 2D Raman intensity imaging was employed over the region marked with the blue box in Figure 2e. As plotted in Figure 2g,h, 2D TERS imaging (8 × 8 spatial grid) maps the $v_{1/6}$ and $v_{1/5}$ domains unambiguously on a large scale, where the cyan and yellow dashed lines mark the borophene edge and the interface between two borophene phases, respectively. These results demonstrate sub-nanoscale Raman responses to the structural phases of pristine borophene, providing a reference for the subsequent identification of organic/borophene heterostructures.

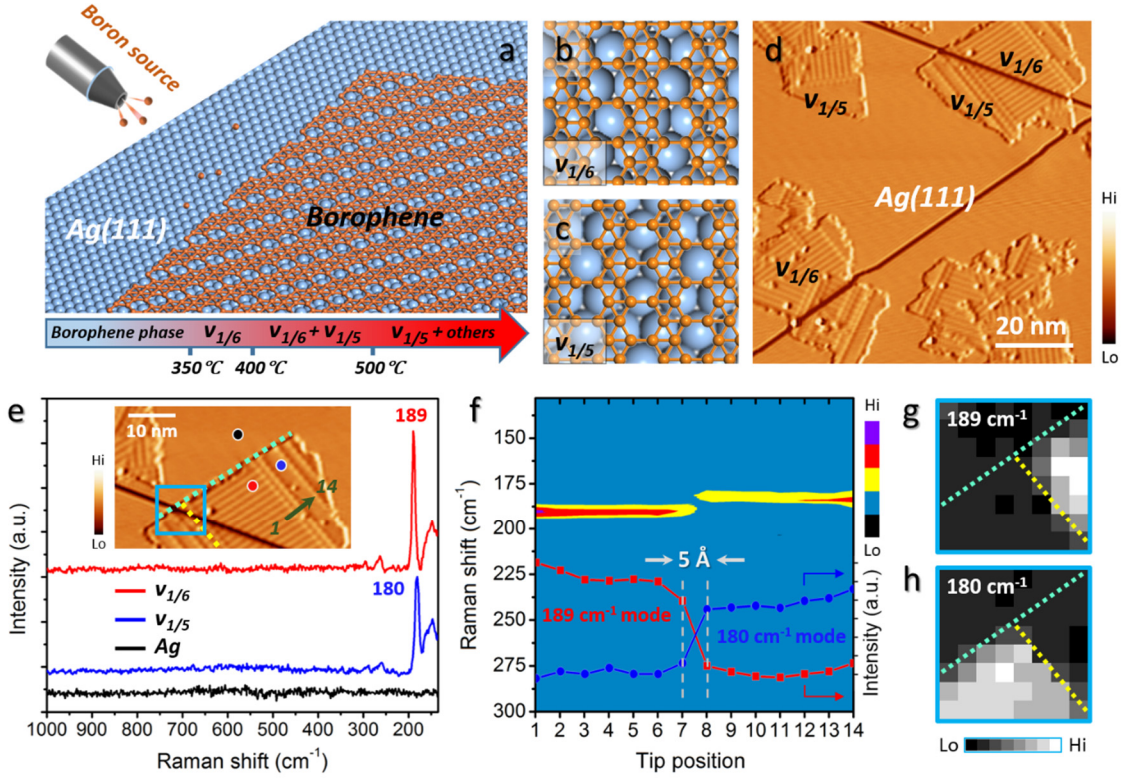

Figure 2. Growth and structural properties of borophene. (a) Schematic illustration of the growth setup, with the bottom diagram showing the growth temperature dependence of borophene structures. Atomic structure models of (b) $v_{1/6}$ and (c) $v_{1/5}$ borophene on Ag(111). (d) Derivative STM topography of sub-monolayer borophene with both $v_{1/6}$ and $v_{1/5}$ phases (2.2 V, 200 pA). (e) TERS spectra (0.5 V, 500 pA, 60 s) acquired on $v_{1/6}$ (red) and $v_{1/5}$ (blue) borophene as well as the Ag(111) surface (black) as shown in the inset STM image (2.2 V, 200 pA). The cyan and yellow dashed lines mark the borophene edge and the interface between $v_{1/6}$ and $v_{1/5}$ domains, respectively. The green line and the blue box indicate the tip trace and the scanned area for the TERS measurements presented in (f) and (g, h), respectively. (f) Spectral evolution for the TERS line scan (0.5 V, 500 pA, 10 s acquisition time per point, 14 points) along the green-line trace marked in (e) with a step size of 5 Å. The corresponding TERS intensity profiles for the 189 cm^{-1} and 180 cm^{-1} Raman modes are superimposed, demonstrating a spatial resolution of 5 Å. 2D intensity mapping (0.5 V, 500 pA, 5 s per pixel, 8 × 8 pixels) of the (g) 189 cm^{-1} and (h) 180 cm^{-1} modes over the region indicated by the blue box in (e).

Self-assembly and interfacial properties of DBP/borophene vertical heterostructures

Having determined the baseline TERS characterization of pristine borophene, we then investigated surface adsorption of DBP. DBP was observed to preferentially adsorb on clean Ag(111) regions prior to adsorption on borophene regions (Figure 1b and Figure S3a), implying a relatively low adsorption enthalpy of DBP on borophene. After fully covering the Ag(111) surface, DBP molecules then adsorbed on borophene with two self-assembled patterns until reaching full coverage of the borophene surface (Figure 1c,d, and Figure S3b,c). To investigate adsorption behaviors of DBP on specific borophene phases, we deposited molecules separately on pure $v_{1/6}$ and pure $v_{1/5}$ borophene samples together with a Ag(111) surface for comparison. As shown in Figure 3a,b, DBP molecules adopt both herringbone-like (H phase; purple) and stripe-like (S phase; green) arrangements on either $v_{1/6}$ or $v_{1/5}$ borophene. The polycrystalline nature of DBP self-assembly on borophene suggests a relatively weak molecule-borophene interaction. In contrast, DBP assembles into a uniform herringbone pattern on the Ag(111) surface (Figure 3c), consistent with a previously reported STM study.[56] Sub-molecular resolution imaging (Figure S4) more clearly depicts the distinct DBP adsorption configurations on borophene and Ag(111) (see detailed discussions in Supplementary Text III in the supporting information).

The interfacial properties of DBP on borophene were then investigated via TERS. Figure 3d presents the corresponding Raman spectra of the molecular samples shown in Figure 3a-c, along with time-dependent density functional theory (TDDFT) simulated spectra for comparison. First, H and S molecular phases on the same borophene structure ($v_{1/6}$ or $v_{1/5}$) exhibit nearly identical spectral profiles (e.g., compare the top purple and green spectra or middle purple and green spectra), indicating the insensitivity of interfacial properties to molecular orientations and geometric arrangements. Second, some slight differences can be observed between the experimental spectra for DBP on different borophene structures, particularly for the high wavenumber region (e.g., compare the two purple spectra), suggesting the possibility to chemically identify DBP molecules adsorbed on different borophene phases. Third, the simulated TERS spectra for DBP on borophene (top and middle black spectra) reproduce the experimentally observed spectral features well, and they appear fairly similar to the calculated TERS spectrum of gas-phase DBP (bottom black), implying a weak van der Waals (vdW) interaction between DBP and borophene. In contrast, the TERS spectrum of DBP on Ag(111) presents few vibrational peaks (bottom blue), especially on the high wavenumber side, which is attributed to a significant electronic interaction between DBP and Ag(111).[56] It is noteworthy that the simulations presented in this work were carried out without taking into account intermolecular interactions and interactions with the Ag substrate, which could be responsible for the small mismatches between measurements and simulations (see theoretical models and more discussions in the supporting information).

Aside from TERS observations of the molecules on surfaces, of particular interest are the prominent Raman signals from the underlying borophene, which are observed in the low wavenumber regions of the TERS spectra of the DBP/borophene samples (i.e., purple and green spectra). Upon adsorption of DBP molecules, $v_{1/6}$ borophene exhibits a similar TERS profile to that of pristine $v_{1/6}$ borophene, but with the characteristic B_{3g}^2 mode blue-shifted from 189 cm^{-1} to 198 cm^{-1}. A similar phonon stiffening effect occurs for the DBP-adsorbed $v_{1/5}$ phase, whose primary B_g^2 peak (194 cm^{-1}) experiences a 14 cm^{-1} shift with

respect to that of the molecule-free $\nu_{1/5}$ (180 cm^{-1}, Figure 2e). In addition to phonon shifts, peak broadening of these two Raman modes has been observed compared to those without molecular adsorption (Figure 2e) particularly for the $\nu_{1/5}$ phase, suggesting structural variations of adsorbed borophene.[65-67]

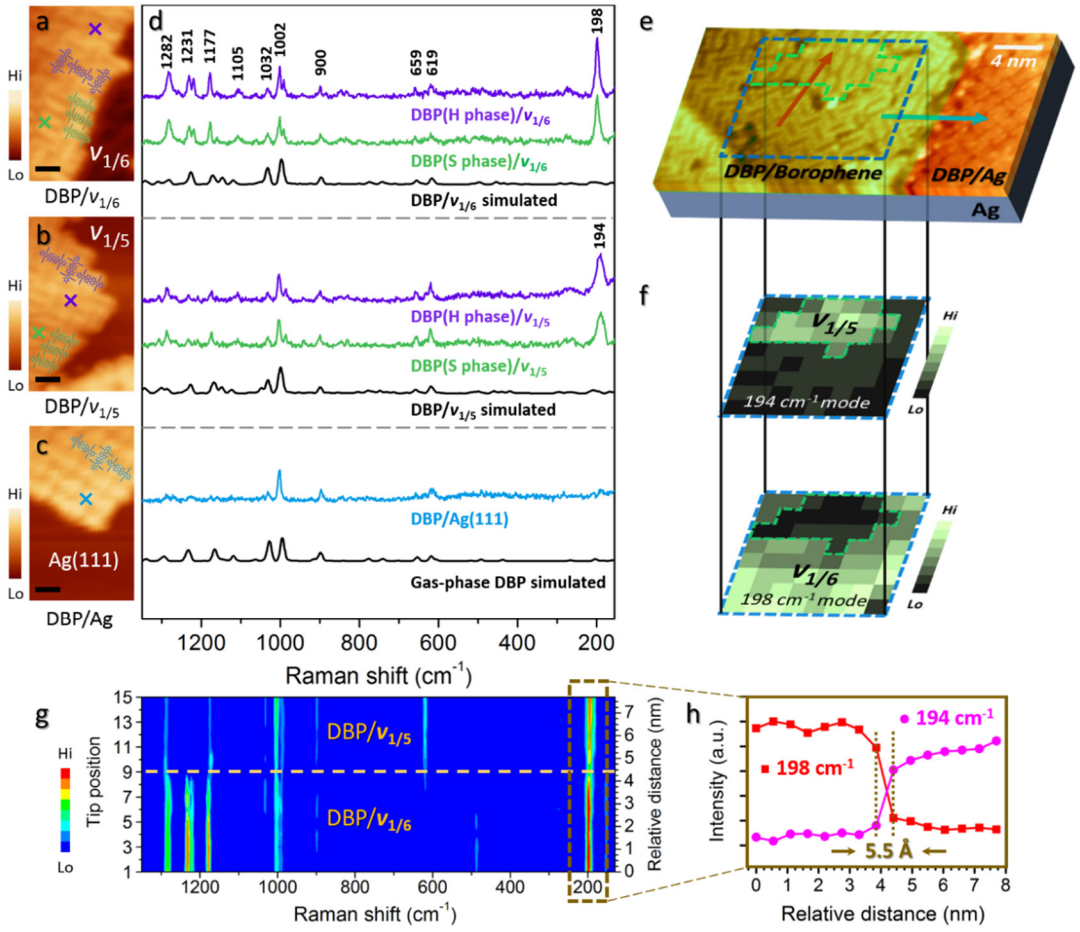

Figure 3. Characterizing DBP/borophene vertical heterostructures via UHV-STM and UHV-TERS. STM images of DBP molecular islands on (a) pure $\nu_{1/6}$ borophene, (b) pure $\nu_{1/5}$ borophene, and (c) clean Ag(111), respectively with molecular models overlaid. The crosses mark the representative sites for the TERS measurements presented in (d) [(a) 1.5 V, 100 pA; (b) 1.5 V, 50 pA; (c) 1.5 V, 200 pA. Scale bars: 2 nm]. (d) TERS spectra (0.5 V, 600 pA, 60 s) acquired on the DBP islands shown in (a-c). For comparison, simulated TERS spectra of DBP are also presented. (e) STM image (2 V, 500 pA) of sub-monolayer mixed-phase borophene covered by a DBP layer. The molecular domains supported on borophene are shaded in yellow green for clarity. The red and blue arrows indicate the tip traces for TERS line scans. The blue square marks the scanned region for 2D TERS imaging, with a green polygon indicating the domain boundary. (f) TERS intensity maps (0.5 V, 500 pA, 8 s, 8 × 8 pixels) of the 194 cm^{-1} and 198 cm^{-1} modes over the region marked with the blue square in (e). (g) Spectral evolution of the TERS line scan (0.5 V, 500 pA, 10 s, 15 points) along the red-line trace in (e) with a step length of 5.5 Å. The dashed line indicates the boundary of DBP-adsorbed $\nu_{1/6}$ and $\nu_{1/5}$ borophene. The brown rectangle highlights the spectral evolution from which (h) the line profiles of Raman intensity for the 198 cm^{-1} and 194 cm^{-1} modes are extracted. The TERS line scan along the blue-line trace in (e) is presented in Figure S5.

UHV-TERS studies to date have exclusively focused on adsorbates themselves (e.g., single molecules or low-dimensional materials) that are supported on rigid and Raman-silent substrates (typically coinage metals). In contrast, experimental demonstrations of UHV-TERS to probe underlying substrate structures and interfacial interactions with hybrid Raman responses are rare. By utilizing the Raman results in Figure 3d, we can not only identify DBP conformations on different borophene phases, but also characterize their effect on the underlying borophene structure, thereby allowing full-scale characterization of the vertical heterointerface. The TERS experiments shown in Figure 3e-h further demonstrate this capability. In particular, Figure 3e depicts a $\nu_{1/6}$ and $\nu_{1/5}$ phase-mixed sub-monolayer borophene sample with all the substrate surfaces fully covered by self-assembled DBP. Owing to the co-existence of two molecular arrangements on either borophene phase, as illustrated in Figure 3a,b, STM characterization alone cannot identify borophene structures underneath according to apparent DBP adsorption geometries. In contrast, the structural distribution of borophene can be visualized by high-resolution 2D TERS imaging. As illustrated in Figure 3f, (8 × 8) sequential TERS measurements over the region indicated with the blue square in Figure 3e have been conducted, and the spectral intensity distributions of the 194 cm^{-1} and 198 cm^{-1} modes have been mapped, respectively. The resulting pair of 2D-mapping images clearly visualizes and distinguishes between the two DBP-covered borophene phases with a sharp domain boundary marked with the green dashed line. Furthermore, in order to demonstrate the spectral evolution across the domain boundary, one-dimensional (1D) TERS measurements were performed along the red-line trace in Figure 3e and plotted in Figure 3g (15 consecutively acquired TERS spectra), providing structural and chemical information describing both DBP and the corresponding borophene substrate. The spectra below and above the dashed line in the middle of Figure 3g can be readily assigned to those of DBP on $\nu_{1/6}$ borophene (positions 1-8) and those of DBP on $\nu_{1/5}$ borophene (positions 9-15) respectively by direct comparison with the reference TERS spectra shown in Figure 3d. Furthermore, we can draw the same conclusion by directly studying the line profiles for the Raman intensity of borophene plotted in Figure 3h. The line profiles for the 198 cm^{-1} and 194 cm^{-1} modes demonstrate that the tip trace along the red line moves from the $\nu_{1/6}$ domain to the $\nu_{1/5}$ domain, with a step length and spatial resolution of 5.5 Å. A similar TERS line scan along the blue-line trace in Figure 3e is displayed in Figure S5. The sharply distinct TERS patterns in the waterfall plot, together with the stark contrast in Raman intensity of borophene in the line profile, demonstrate that the left molecular domain along the tip trace is on top of borophene while the right one is on top of the Ag surface. Note that, when the line scans were performed along different orientations of the $\nu_{1/6}$ domain (the first halves of the red and blue arrows), no strain variations were observed although anisotropic strain behaviors could reasonably be expected given the structural anisotropy of borophene (see more discussions in Supplementary Text IV in the supporting information).

To better understand the origin of the phonon shift of DBP-adsorbed borophene, we turn to a theoretical treatment of the DBP/borophene interface (see theoretical models in the supporting information). The energetically favorable configurations are presented in Figure 4a,b (side view; see top view in Figure S6). Note that the calculated adsorption conformations and energies are insensitive to molecular orientations on either borophene phase, further indicating the weak binding of DBP to the borophene surface. However, this weak interfacial coupling can still bring about an observable morphological change in

borophene due to its high lattice flexibility. As shown in the simulated structures (Figure 4a,b), the gentle undulations of the borophene lattice (as indicated by the blue arrows) under the molecules are visible on closer inspection, which are in sharp contrast to the fairly flat surfaces of pristine borophene as presented in Figure 4c,d. Subsequently, the phonon vibration of adsorbed borophene was investigated via DFT calculations. Figure 4e-h schematically shows the atomic displacements of the B_{3g}^2 mode in the $\nu_{1/6}$ phase and the B_g^2 mode in the $\nu_{1/5}$ phase without and with molecular adsorption, respectively (side view; molecules are not shown). Evidently, the phonon wave vectors otherwise oriented perpendicular to the borophene planes (i.e., parallel to the Z-axial plasmonic field; Figure 4e,f) are perturbed after DBP adsorbs on top of either $\nu_{1/6}$ or $\nu_{1/5}$ borophene (Figure 4g,h). This perturbation to the out-of-plane vibrations accounts for the frequency shifts of the corresponding Raman modes. The Raman shifts of the B_{3g}^2 mode ($\nu_{1/6}$) and B_g^2 mode ($\nu_{1/5}$) under different conditions are summarized in Table S1 (Supporting Information), which shows good agreement between experiment and theory.

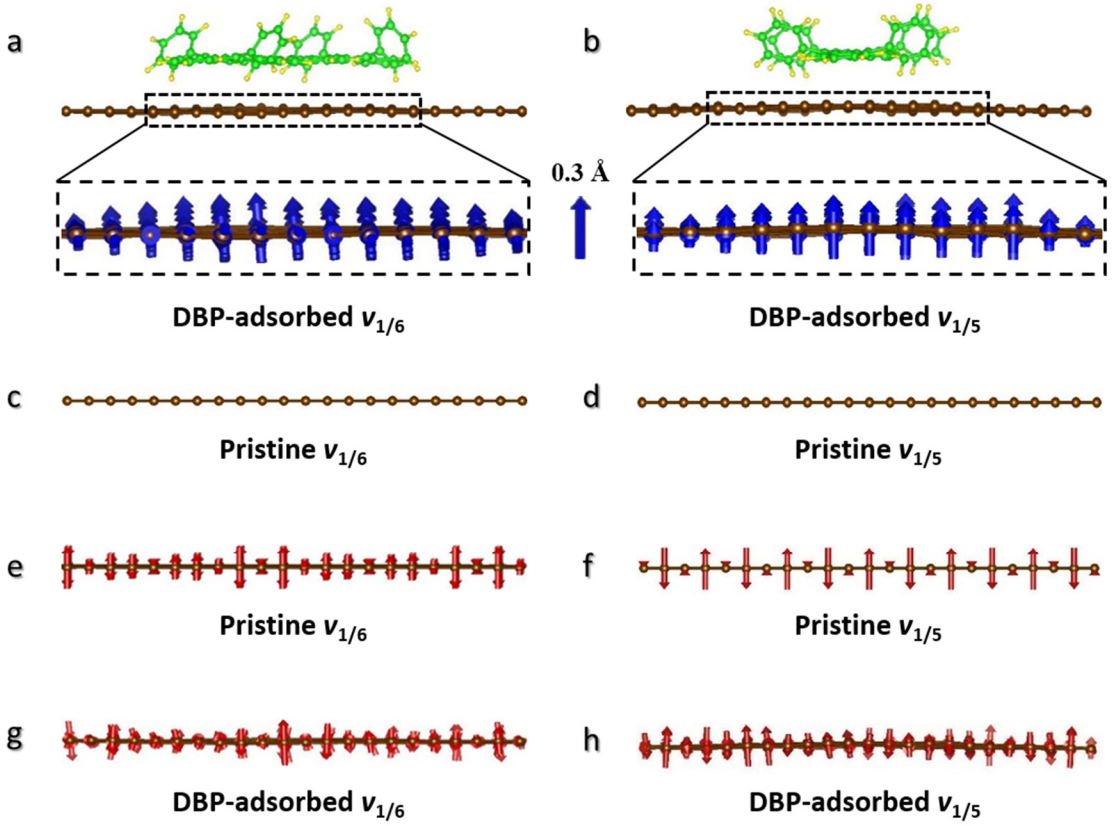

Figure 4. Theoretically investigating vertical interfacial interactions between DBP and borophene. Side view of DBP adsorption configurations on (a) $\nu_{1/6}$ borophene and (b) $\nu_{1/5}$ borophene with the blue arrows added to indicate boron atomic displacements. Side view of pristine (c) $\nu_{1/6}$ borophene and (d) $\nu_{1/5}$ borophene. Side view of atomic displacements of the B_{3g}^2 Raman mode in the $\nu_{1/6}$ phase (e) without and (g) with DBP adsorption. Side view of atomic displacements of the B_g^2 Raman mode in the $\nu_{1/5}$ phase (f) without and (h) with DBP adsorption. Molecules are not shown in (g) and (h) for clarity.

In addition to lattice undulations, in-plane lattice deformation of adsorbed borophene was observed. Taking adsorbed $v_{1/6}$ borophene as an example (Figure 5a,b), boron atomic displacements are readily visible underneath the molecule, as indicated by the blue arrows (the molecule is removed for clarity in Figure 5b). An apparent observation is that all of the atomic displacements are oriented in plane towards the molecule and that the atomic displacements are largest near the molecule. The net result is that the boron lattice under the molecule is distorted upward and strained compressively. These observations, together with the measured blue shift of phonon modes for adsorbed borophene, are consistent with studies of the strain dependence of Raman responses of graphene and other 2D materials – namely, that compressive strains generally induce phonon stiffening while tensile strains lead to phonon softening.[68-70]

Molecular adsorption-induced localized interfacial strains

For a full-coverage DBP/borophene heterostructure, the aforementioned interfacial properties are uniform and isotropic on a large scale. However, a close examination of the edge of a DBP/borophene interface (Figure 5b) indicates that, the borophene lattice deformation can extend beyond the molecular region – a behavior like "strain spillover" – if only a single molecule or molecular island is involved, consistent with the excellent mechanical stretchability and bending flexibility of borophene sheets. Considering the sensitive Raman response to structural variations, we investigated the correlation of the Raman shift and lattice dimension for borophene with a simplified structural model, as shown in Figure 5c, which involves uniform stretching of a $v_{1/6}$ borophene lattice (i.e., biaxial tensile strain). Based on this model, the relationship between the frequency shift of the B_{3g}^2 mode and applied lattice strain was obtained. As plotted in Figure 5c, the Raman shift decreases monotonically with lattice expansion, where, for instance, 0.6% tensile strain leads to a frequency shift of -6 cm^{-1} with respect to the Raman shift of strain-free borophene. Note that similar effects of strain on phonon response have been revealed in other 2D materials, such as graphene, hexagonal boron nitride, phosphorene, and transition metal dichalcogenides.[68-72]

Following the above theoretical analysis, UHV-TERS was employed to experimentally identify and characterize these subtle and highly localized interfacial strain effects. Specifically, a DBP molecular island was deposited on a pure $v_{1/6}$ borophene monolayer, as shown in Figure 5d, exposing a sharp DBP-borophene interface. When the tip is positioned far away from the DBP island (green spot), a spectrum (green) dominated by a 190 cm^{-1} peak is obtained, which corresponds to the characteristic of pristine borophene (the tiny deviation from 189 cm^{-1} shown in Figure 2e may result from measurement error). Notably, as the tip moves close to the island edge (red spot), a distinctive spectrum (red) is observed with a relatively weak peak located at 184 cm^{-1}. This new spectrum is in sharp contrast to that of either pristine or DBP-adsorbed borophene. The latter is nicely reproduced in the blue spectrum upon localization of the tip on the DBP island (blue spot). Note that, with respect to the 190 cm^{-1} peak of pristine borophene, the new spectrum undergoes an opposite phonon shift (red shift) to that of adsorbed borophene (blue shift), implying distinct structural properties between the edge and the interior of adsorbed borophene. To see more clearly how the TERS spectra evolve across the DBP-borophene interface, we plot the corresponding 1D TERS spectra in Figure 5e that were acquired consecutively along the yellow-line trace shown in Figure 5d with a step size of 5 Å. The

spectra on positions 1-3 reproduce the TERS features of pristine $v_{1/6}$ borophene as displayed in Figure 2e, while those on positions 7-9 can be assigned to TERS spectra of adsorbed $v_{1/6}$ borophene as presented in Figure 3d. Between these well-defined spectra, new distinct spectra are observed on positions 4-6 with their primary peaks 6 cm^{-1} red-shifted with respect to those of pristine borophene. This spectral analysis suggests a region of 1-1.5 nm in length beyond the molecular island for these new features. These intermediate spectra apparently originate from the highly localized strain in immediate proximity to the adsorbed borophene.

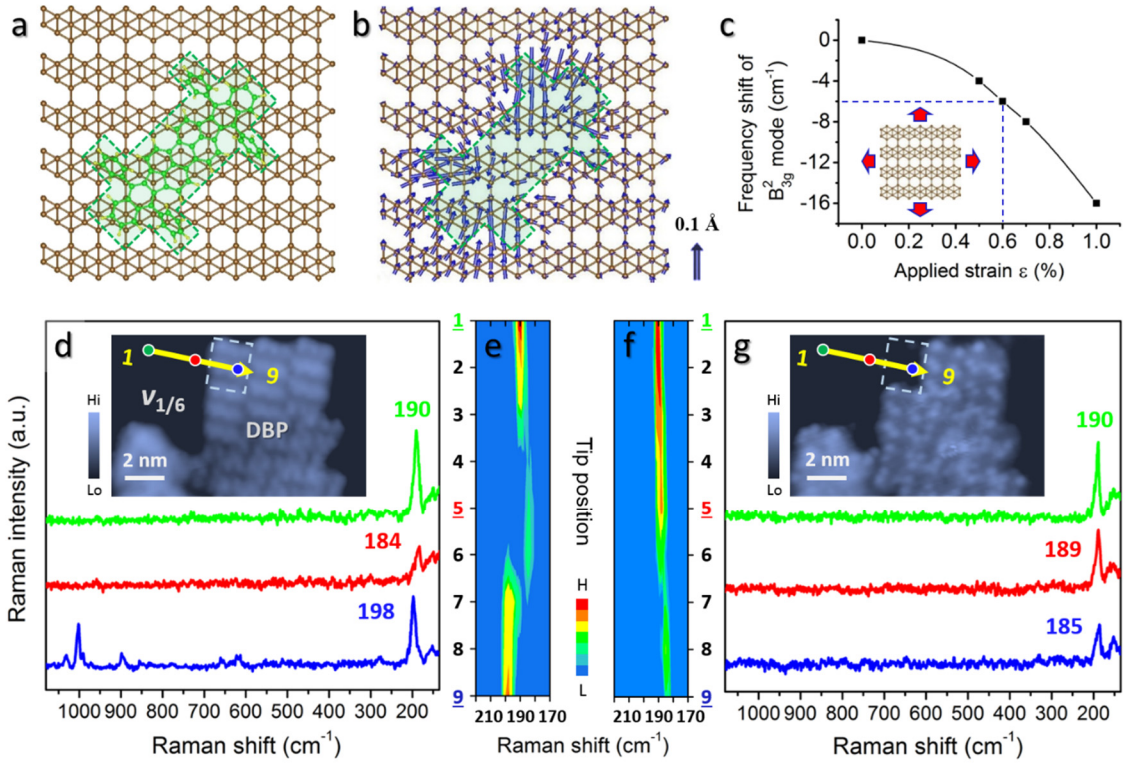

Figure 5. Probing molecular adsorption-induced interfacial strains. (a) Top view of the adsorption configuration for DBP on $v_{1/6}$ borophene with a green contour superimposed. (b) Same illustration as (a), but with the blue arrows added to denote boron atomic displacements. The molecular model has been removed for clarity, leaving the green contour to indicate the position of the DBP molecule. (c) Correlation between frequency shift of the B^2_{3g} mode and lattice strain of $v_{1/6}$ borophene. Inset: Corresponding theoretical model involving biaxial tensile strain applied to the borophene lattice. (d) TERS spectra (0.5 V, 500 pA, 10 s) acquired at the sites marked with the colored spots in the inset STM image (1.5 V, 200 pA). The yellow arrow indicates the tip trace for the 1D TERS measurements shown in (e). The dashed-line box marks the two molecules to be removed. (e) Spectral evolution for the 1D TERS measurements (0.5 V, 500 pA, 10 s per point, 9 points) along the yellow-line trace displayed in the inset of (d) with a step size of 0.5 nm. (f) Spectral evolution for the 1D TERS measurements (0.5 V, 500 pA, 10 s per point, 9 points) along the yellow-line trace displayed in the inset of (g) with a step size of 0.5 nm. (g) TERS spectra (0.5 V, 500 pA, 10 s) acquired on the same sample as (d), but with two DBP molecules removed as indicated with the dashed-line box in the inset (1.2 V, 100 pA).

Atomic manipulation of interfacial structures and interactions is critical for understanding and controlling the performance of 2D heterostructured systems. Low-temperature STM has been demonstrated to be a powerful tool for the precise manipulation of atoms and molecules on surfaces and the artificial design of desired nanostructures.[54,73-75] The STM tip, when used for molecular manipulations, is able to modify molecular structures and properties, as well as tune their interactions with local environments. Here, a protocol coupling molecular manipulations with TERS investigations is performed in order to gain deeper insight into the nature of interfacial strains (see experimental details in Supplementary Text V in the supporting information). Briefly, owing to the rather weak DBP-borophene attraction, we can remove molecules from molecular monolayers, particularly at boundaries and corners of molecular islands by dragging the molecules with a scanning STM tip that is approached close to the sample (Figure S7). Figure 5g illustrates one sample created from the molecular island shown in Figure 5d, where two DBP molecules within the dashed-line box have been removed. TERS measurements were then carried out on this new DBP-borophene interface. The line scan spectra are presented in Figure 5f, with the yellow tip trace shown in the inset of Figure 5g. Two prominent observations can be made by comparing the spectral plots displayed in Figure 5e,f. First, that borophene previously located at the interface with DBP (positions 4-6 in Figure 5f) features the same spectral profile as that of strain-free borophene (positions 1-3 in Figure 5f) in response to the strain release via molecular manipulation. Second, the 198 cm^{-1} peaks acquired above the molecular island (positions 7-9 in Figure 5e) disappear after removal of those DBP molecules (positions 7-9 in Figure 5f), which in turn confirms that the 198 cm^{-1} mode stems from the blue-shifted B_{3g}^2 mode of $v_{1/6}$ borophene induced by molecular adsorption.

We highlight the spectra of interest acquired at the same positions following molecular manipulation for a direct comparison of Figure 5d and 5g. As expected, the spectrum (green) collected on the green spot exhibits the spectral features of pristine $v_{1/6}$ borophene in both instances and thus reflects a strain-free nature for this region of borophene. This observation indicates that the removal of DBP molecules has no effect on the structural properties of the borophene far away from the molecular island. More importantly, the absence of molecular signals following the molecular manipulation confirms the cleanliness of the STM tip. Otherwise, strong Raman peaks stemming from a DBP-contaminated tip would be observed (Figure S8; see detailed discussions in Supplementary Text VI in the supporting information). Prior to molecular manipulation, the spectrum (red) acquired on the red spot in Figure 5d has a dominant peak at 184 cm^{-1}, a feature that can be identified as characteristic of borophene adjacent to an adsorbed DBP molecular island. Following the removal of the DBP molecules, the spectrum acquired at the same tip position (Figure 5g red) shows a dominant peak located at 189 cm^{-1}, quite akin to that of pristine borophene. Further, moving the tip closer to the molecular island onto the newly formed borophene-DBP interface (i.e., the blue spot) yields a spectrum (Figure 5g blue) that is closely similar to the red spectrum in Figure 5d acquired at the previous borophene-DBP interface.

These TERS observations provide solid evidence that the newly revealed 184 cm^{-1} peak originates from the molecular adsorption-induced interfacial strain. Significantly, the removal of molecules results in the relaxation of local strain and thus the recovery of intrinsic TERS features of pristine borophene, as demonstrated by the comparison of

measurements on the red spots before and after molecular manipulation. Furthermore, the strain-induced TERS response can be observed again at the new borophene-molecule interface. According to the relationship between phonon frequency shift and lattice strain established in Figure 5c, the measured frequency shift of -6 cm^{-1} here (from 190 cm^{-1} to 184 cm^{-1}) corresponds to a tensile strain of ~0.6% (as indicated with blue dashed lines in Figure 5c). Therefore, STM-controlled molecular manipulation combined with TERS measurements enables local tuning and interrogation of delicate interfacial strains with exceptional chemical spatial resolution. Furthermore, locally induced strain distributions of borophene can be visualized via 2D TERS mapping. As illustrated in Figure S10, Raman intensities at three frequencies of 190 cm^{-1}, 184 cm^{-1}, and 198 cm^{-1} are mapped, respectively, over a region on the DBP-borophene border. The intensity mapping images for the 198 cm^{-1} and 184 cm^{-1} modes reveal the strain distributions of the adsorbed borophene and its vicinity, respectively. In particular, the latter is found to be localized within ~1.5 nm in length away from the molecular island, which is in agreement with the preceding analysis. Such high sensitivity 2D TERS mapping is expected to be a powerful tool for probing and analyzing extremely localized interfacial properties in other 2D materials and heterostructures.

Conclusion

In summary, by virtue of the sensitive chemical recognition and ultrahigh spatial resolution of UHV-TERS, we have studied the correlation of local structural heterogeneities with angstrom-scale Raman responses in DBP/borophene heterostructures, thereby depicting an informative picture of DBP-borophene interactions. DBP adsorption can result in the undulation and compression of the borophene lattice underneath molecules, which can be detected via TERS band shifts in response to the modified lattice vibration (phonon). Furthermore, molecular adsorption leads to the generation of a subtle tensile strain in borophene with magnitudes as small as ~0.6%, which is highly localized in close proximity to the adsorbed borophene with a typical range of 1-1.5 nm. With more molecular deposition and increases in the size of DBP islands, this strain on the frontier will propagate outwards along the perimeter of molecular islands and eventually disappear for a full-coverage DBP/borophene sample such as the one shown in Figure 3e. This scenario indicates exceptional structural compliance and property tunability of borophene when integrated into heterostructures. These unique qualities could be further enhanced and modulated by its structural anisotropy and polymorphism.

As the first demonstration of an organic/borophene vertical heterostructure, this work suggests a prototypical and generalizable experimental strategy for strain engineering of 2D materials via organic modification on top, in contrast to the conventional approach by controlling the deformation of the substrate. Besides enabling the introduction of long-term and reversible strains, molecular adsorption and STM tip manipulation offer a powerful means to achieve atomic control of strain and strain-coupled properties, such as phonon vibration, electronic structure, thermal conductivity, carrier mobility, and chemical reactivity. In particular, bandgap structure and transport properties can be modified via strain engineering and further tailored in virtue of tunable anisotropy of borophene polymorphs,[76] which suggests tremendous promise for (opto-)electronic applications.[77] Moreover, superconducting transition temperature T_c can be dramatically tuned by subtly changing lattice parameters. For example, compressively strained $\nu_{1/6}$ borophene, as

realized in this study via molecular adsorption, has been theoretically predicted to possess enhanced superconducting T_c, thereby opening up an opportunity to experimentally observe superconductivity in borophene.[78] In addition, the ability to simultaneously provide chemical fingerprints of adsorbed molecules and topographic information of underlying borophene demonstrates UHV-STM-TERS can go beyond structural characterization and chemical identification on the surface, allowing atomic-scale interrogation of the local nature of interfacial properties in complex heterostructures.

Present Addresses:

[#]X.L: LASSP, Department of Physics, Cornell University, Ithaca NY 14850, United States.

Notes:

The authors declare no competing financial interest.

Supporting Information

Materials and methods, adsorption configurations of DBP on borophene, STM topographs of DBP-borophene heterostructures, topographic evolution and sub-molecular resolution geometries of DBP adsorption, additional TERS line scan, anisotropic strains in borophene, top view of DBP adsorption models on borophene, molecular manipulation on borophene with STM tip, tip-contamination induced Raman spectra, TERS spectra acquired with a contamination-free tip, TERS mapping of interfacial strains of adsorbed borophene, Raman shifts of B_{3g}^2 mode ($\nu_{1/6}$) and B_g^2 mode ($\nu_{1/5}$) under different conditions.

Acknowledgements

N.J. acknowledges support from the National Science Foundation (CHE-1944796). X.Z. acknowledges support from the National Science Foundation (DMR-1828019). M.C.H. acknowledges support from the Office of Naval Research (N00014-17-1-2993) and the National Science Foundation (DMR-1720139).

References

1. Mannix, A. J.; Zhou, X. F.; Kiraly, B.; Wood, J. D.; Alducin, D.; Myers, B. D.; Liu, X. L.; Fisher, B. L.; Santiago, U.; Guest, J. R.; Yacaman, M. J.; Ponce, A.; Oganov, A. R.; Hersam, M. C.; Guisinger, N. P., Synthesis of borophenes: Anisotropic, two-dimensional boron polymorphs. *Science* 2015, *350* (6267), 1513-1516.
2. Feng, B. J.; Zhang, J.; Zhong, Q.; Li, W. B.; Li, S.; Li, H.; Cheng, P.; Meng, S.; Chen, L.; Wu, K. H., Experimental realization of two-dimensional boron sheets. *Nat. Chem.* 2016, *8* (6), 564-569.
3. Liu, X. L.; Wang, L. Q.; Li, S. W.; Rahn, M. S.; Yakobson, B. I.; Hersam, M. C., Geometric imaging of borophene polymorphs with functionalized probes. *Nat. Commun.* 2019, *10*, 1642.
4. Liu, X. L.; Zhang, Z. H.; Wang, L. Q.; Yakobson, B. I.; Hersam, M. C., Intermixing and periodic self-assembly of borophene line defects. *Nat. Mater.* 2018, *17* (9), 783-788.
5. Penev, E. S.; Bhowmick, S.; Sadrzadeh, A.; Yakobson, B. I., Polymorphism of Two-Dimensional Boron. *Nano Lett.* 2012, *12* (5), 2441-2445.
6. Liu, Y. Y.; Penev, E. S.; Yakobson, B. I., Probing the Synthesis of Two-Dimensional Boron by First-Principles Computations. *Angew. Chem. Int. Ed.* 2013, *52* (11), 3156-3159.
7. Penev, E. S.; Kutana, A.; Yakobson, B. I., Can Two-Dimensional Boron Superconduct? *Nano Lett.* 2016, *16* (4), 2522-2526.
8. Feng, B. J.; Sugino, O.; Liu, R. Y.; Zhang, J.; Yukawa, R.; Kawamura, M.; Iimori, T.; Kim, H.; Hasegawa, Y.; Li, H.; Chen, L.; Wu, K. H.; Kumigashira, H.; Komori, F.; Chiang, T. C.; Meng, S.; Matsuda, I., Dirac Fermions in Borophene. *Phys. Rev. Lett.* 2017, *118* (9), 096401.
9. Li, Q.; Kolluru, V. S. C.; Rahn, M. S.; Schwenker, E.; Li, S.; Hennig, R. G.; Darancet, P.; Chan, M. K. Y.; Hersam, M. C., Synthesis of borophane polymorphs through hydrogenation of borophene. *Science* 2021, *371* (6534), 1143-1148.
10. Mannix, A. J.; Zhang, Z. H.; Guisinger, N. P.; Yakobson, B. I.; Hersam, M. C., Borophene as a prototype for synthetic 2D materials development. *Nat. Nanotechnol.* 2018, *13* (6), 444-450.
11. Wang, Z. Q.; Lu, T. Y.; Wang, H. Q.; Feng, Y. P.; Zheng, J. C., Review of borophene and its potential applications. *Front. Phys.* 2019, *14* (3), 33403.
12. Xie, S.-Y.; Wang, Y.; Li, X.-B., Flat Boron: A New Cousin of Graphene. *Adv. Mater.* 2019, *31* (36), 1900392.
13. Zhang, Z. H.; Yang, Y.; Penev, E. S.; Yakobson, B. I., Elasticity, Flexibility, and Ideal Strength of Borophenes. *Adv. Funct. Mater.* 2017, *27* (9), 1605059.
14. Mortazavi, B.; Rahaman, O.; Dianat, A.; Rabczuk, T., Mechanical responses of borophene sheets: a first-principles study. *Phys. Chem. Chem. Phys.* 2016, *18* (39), 27405-27413.
15. Zhang, Z. H.; Mannix, A. J.; Hu, Z. L.; Kiraly, B.; Guisinger, N. P.; Hersam, M. C.; Yakobson, B. I., Substrate-Induced Nanoscale Undulations of Borophene on Silver. *Nano Lett.* 2016, *16* (10), 6622-6627.
16. Liu, X. L.; Wei, Z. H.; Balla, I.; Mannix, A. J.; Guisinger, N. P.; Luijten, E.; Hersam, M. C., Self-assembly of electronically abrupt borophene/organic lateral heterostructures. *Sci. Adv.* 2017, *3* (2), e1602356.
17. Liu, X. L.; Hersam, M. C., Borophene-graphene heterostructures. *Sci. Adv.* 2019, *5* (10), eaax6444.
18. Lee, C. H.; Schiros, T.; Santos, E. J. G.; Kim, B.; Yager, K. G.; Kang, S. J.; Lee, S.; Yu, J.; Watanabe, K.; Taniguchi, T.; Hone, J.; Kaxiras, E.; Nuckolls, C.; Kim, P.,

Epitaxial Growth of Molecular Crystals on van der Waals Substrates for High-Performance Organic Electronics. *Adv. Mater.* **2014, *26* (18), 2812-2817.**

19. Lee, W. H.; Park, J.; Sim, S. H.; Lim, S.; Kim, K. S.; Hong, B. H.; Cho, K., Surface-Directed Molecular Assembly of Pentacene on Monolayer Graphene for High-Performance Organic Transistors. *J. Am. Chem. Soc.* **2011, *133* (12), 4447-4454.**

20. Colson, J. W.; Woll, A. R.; Mukherjee, A.; Levendorf, M. P.; Spitler, E. L.; Shields, V. B.; Spencer, M. G.; Park, J.; Dichtel, W. R., Oriented 2D Covalent Organic Framework Thin Films on Single-Layer Graphene. *Science* **2011, *332* (6026), 228-231.**

21. Jariwala, D.; Howell, S. L.; Chen, K. S.; Kang, J. M.; Sangwan, V. K.; Filippone, S. A.; Turrisi, R.; Marks, T. J.; Lauhon, L. J.; Hersam, M. C., Hybrid, Gate-Tunable, van der Waals p-n Heterojunctions from Pentacene and MoS2. *Nano Lett.* **2016, *16* (1), 497-503.**

22. Wang, Q. H.; Hersam, M. C., Room-temperature molecular-resolution characterization of self-assembled organic monolayers on epitaxial graphene. *Nat. Chem.* **2009, *1* (3), 206-211.**

23. Ryder, C. R.; Wood, J. D.; Wells, S. A.; Yang, Y.; Jariwala, D.; Marks, T. J.; Schatz, G. C.; Hersam, M. C., Covalent functionalization and passivation of exfoliated black phosphorus via aryl diazonium chemistry. *Nat. Chem.* **2016, *8* (6), 597-602.**

24. Mao, H. Y.; Lu, Y. H.; Lin, J. D.; Zhong, S.; Wee, A. T. S.; Chen, W., Manipulating the electronic and chemical properties of graphene via molecular functionalization. *Prog. Surf. Sci.* **2013, *88* (2), 132-159.**

25. Novoselov, K. S.; Mishchenko, A.; Carvalho, A.; Neto, A. H. C., 2D materials and van der Waals heterostructures. *Science* **2016, *353* (6298), aac9439.**

26. Jariwala, D.; Marks, T. J.; Hersam, M. C., Mixed-dimensional van der Waals heterostructures. *Nat. Mater.* **2017, *16* (2), 170-181.**

27. Liu, Y.; Weiss, N. O.; Duan, X. D.; Cheng, H. C.; Huang, Y.; Duan, X. F., Van der Waals heterostructures and devices. *Nat. Rev. Mater.* **2016, *1* (9), 16042.**

28. Zhang, W.; Wang, Q.; Chen, Y.; Wang, Z.; Wee, A. T. S., Van der Waals stacked 2D layered materials for optoelectronics. *2d Mater* **2016, *3* (2), 022001.**

29. Zhang, C.; Li, M.-Y.; Tersoff, J.; Han, Y.; Su, Y.; Li, L.-J.; Muller, D. A.; Shih, C.-K., Strain distributions and their influence on electronic structures of WSe2–MoS2 laterally strained heterojunctions. *Nat. Nanotechnol.* **2018, *13* (2), 152-158.**

30. Li, B.; Huang, L.; Zhong, M.; Li, Y.; Wang, Y.; Li, J.; Wei, Z., Direct Vapor Phase Growth and Optoelectronic Application of Large Band Offset SnS2/MoS2 Vertical Bilayer Heterostructures with High Lattice Mismatch. *Advanced Electronic Materials* **2016, *2* (11), 1600298.**

31. Oakes, L.; Carter, R.; Hanken, T.; Cohn, A. P.; Share, K.; Schmidt, B.; Pint, C. L., Interface strain in vertically stacked two-dimensional heterostructured carbon-MoS2 nanosheets controls electrochemical reactivity. *Nat. Commun.* **2016, *7* (1), 11796.**

32. Song, I.; Goh, J. S.; Lee, S.-H.; Jung, S. W.; Shin, J. S.; Yamane, H.; Kosugi, N.; Yeom, H. W., Realization of a Strained Atomic Wire Superlattice. *ACS Nano* **2015, *9* (11), 10621-10627.**

33. Yin, H.; Zheng, L.-Q.; Fang, W.; Lai, Y.-H.; Porenta, N.; Goubert, G.; Zhang, H.; Su, H.-S.; Ren, B.; Richardson, J. O.; Li, J.-F.; Zenobi, R., Nanometre-scale spectroscopic visualization of catalytic sites during a hydrogenation reaction on a Pd/Au bimetallic catalyst. *Nature Catalysis* **2020, *3* (10), 834-842.**

34. Stadler, J.; Schmid, T.; Zenobi, R., Nanoscale Chemical Imaging of Single-Layer Graphene. *ACS Nano* **2011, *5* (10), 8442-8448.**

35. Zhong, J. H.; Jin, X.; Meng, L. Y.; Wang, X.; Su, H. S.; Yang, Z. L.; Williams, C. T.; Ren, B., Probing the electronic and catalytic properties of a bimetallic surface with 3 nm resolution. *Nat. Nanotechnol.* **2017, *12* (2), 132-136.**

36. **Pfisterer, J. H. K.; Baghernejad, M.; Giuzio, G.; Domke, K. F., Reactivity mapping of nanoscale defect chemistry under electrochemical reaction conditions. *Nat. Commun.* 2019, *10*, 5702.**
37. **Sabanes, N. M.; Ohto, T.; Andrienko, D.; Nagata, Y.; Domke, K. F., Electrochemical TERS Elucidates Potential-Induced Molecular Reorientation of Adenine/Au(111). *Angew. Chem. Int. Ed.* 2017, *56* (33), 9796-9801.**
38. **Mahapatra, S.; Li, L.; Schultz, J. F.; Jiang, N., Tip-enhanced Raman spectroscopy: Chemical analysis with nanoscale to angstrom scale resolution. *J. Chem. Phys.* 2020, *153* (1), 010902.**
39. **Schultz, J. F.; Mahapatra, S.; Li, L.; Jiang, N., The Expanding Frontiers of Tip-Enhanced Raman Spectroscopy. *Appl. Spectrosc.* 2020, *74*, 1313-1340.**
40. **Schultz, J. F.; Li, S.; Jiang, S.; Jiang, N., Optical scanning tunneling microscopy based chemical imaging and spectroscopy. *J. Phys.: Condens. Matter* 2020, *32*, 463001.**
41. **Steidtner, J.; Pettinger, B., High-resolution microscope for tip-enhanced optical processes in ultrahigh vacuum. *Rev. Sci. Instrum.* 2007, *78* (10), 103104.**
42. **Pozzi, E. A.; Goubert, G.; Chiang, N.; Jiang, N.; Chapman, C. T.; McAnally, M. O.; Henry, A.-I.; Seideman, T.; Schatz, G. C.; Hersam, M. C.; Duyne, R. P. V., Ultrahigh-Vacuum Tip-Enhanced Raman Spectroscopy. *Chem. Rev.* 2017, *117* (7), 4961-4982.**
43. **Lee, J.; Crampton, K. T.; Tallarida, N.; Apkarian, V. A., Visualizing vibrational normal modes of a single molecule with atomically confined light. *Nature* 2019, *568* (7750), 78-82.**
44. **Chiang, N. H.; Chen, X.; Goubert, G.; Chulhai, D. V.; Chen, X.; Pozzi, E. A.; Jiang, N.; Hersam, M. C.; Seideman, T.; Jensen, L.; Van Duyne, R. P., Conformational Contrast of Surface-Mediated Molecular Switches Yields Angstrom-Scale Spatial Resolution in Ultrahigh Vacuum Tip-Enhanced Raman Spectroscopy. *Nano Lett.* 2016, *16* (12), 7774-7778.**
45. **Jiang, N.; Chiang, N. H.; Madison, L. R.; Pozzi, E. A.; Wasielewski, M. R.; Seideman, T.; Ratner, M. A.; Hersam, M. C.; Schatz, G. C.; Van Duyne, R. P., Nanoscale Chemical Imaging of a Dynamic Molecular Phase Boundary with Ultrahigh Vacuum Tip-Enhanced Raman Spectroscopy. *Nano Lett.* 2016, *16* (6), 3898-3904.**
46. **Jiang, N.; Foley, E. T.; Klingsporn, J. M.; Sonntag, M. D.; Valley, N. A.; Dieringer, J. A.; Seideman, T.; Schatz, G. C.; Hersam, M. C.; Van Duyne, R. P., Observation of multiple vibrational modes in ultrahigh vacuum tip-enhanced Raman spectroscopy combined with molecular-resolution scanning tunneling microscopy. *Nano Lett.* 2012, *12* (10), 5061-7.**
47. **Mahapatra, S.; Ning, Y. Y.; Schultz, J. F.; Li, L. F.; Zhang, J. L.; Jiang, N., Angstrom Scale Chemical Analysis of Metal Supported Trans- and Cis-Regioisomers by Ultrahigh Vacuum Tip-Enhanced Raman Mapping. *Nano Lett.* 2019, *19* (5), 3267-3272.**
48. **Schultz, J. F.; Li, L.; Mahapatra, S.; Shaw, C.; Zhang, X.; Jiang, N., Defining Multiple Configurations of Rubrene on a Ag(100) Surface with 5 Å Spatial Resolution via Ultrahigh Vacuum Tip-Enhanced Raman Spectroscopy. *J. Phys. Chem. C* 2020, *124* (4), 2420-2426.**
49. **Zhang, R.; Zhang, Y.; Dong, Z. C.; Jiang, S.; Zhang, C.; Chen, L. G.; Zhang, L.; Liao, Y.; Aizpurua, J.; Luo, Y.; Yang, J. L.; Hou, J. G., Chemical mapping of a single molecule by plasmon-enhanced Raman scattering. *Nature* 2013, *498* (7452), 82-86.**
50. **Jiang, S.; Zhang, Y.; Zhang, R.; Hu, C.; Liao, M.; Luo, Y.; Yang, J.; Dong, Z.; Hou, J. G., Distinguishing adjacent molecules on a surface using plasmon-enhanced Raman scattering. *Nat. Nanotechnol.* 2015, *10* (10), 865-869.**

51. **Jaculbia, R. B.; Imada, H.; Miwa, K.; Iwasa, T.; Takenaka, M.; Yang, B.; Kazuma, E.; Hayazawa, N.; Taketsugu, T.; Kim, Y., Single-molecule resonance Raman effect in a plasmonic nanocavity.** ***Nat. Nanotechnol.*** **2020,** ***15*** **(2), 105-110.**
52. **Liu, S.; Müller, M.; Sun, Y.; Hamada, I.; Hammud, A.; Wolf, M.; Kumagai, T., Resolving the Correlation between Tip-Enhanced Resonance Raman Scattering and Local Electronic States with 1 nm Resolution.** ***Nano Lett.*** **2019,** ***19*** **(8), 5725-5731.**
53. **Chiang, N.; Jiang, N.; Madison, L. R.; Pozzi, E. A.; Wasielewski, M. R.; Ratner, M. A.; Hersam, M. C.; Seideman, T.; Schatz, G. C.; Van Duyne, R. P., Probing Intermolecular Vibrational Symmetry Breaking in Self-Assembled Monolayers with Ultrahigh Vacuum Tip-Enhanced Raman Spectroscopy.** ***J. Am. Chem. Soc.*** **2017,** ***139*** **(51), 18664-18669.**
54. **Liao, M. H.; Jiang, S.; Hu, C. R.; Zhang, R.; Kuang, Y. M.; Zhu, J. Z.; Zhang, Y.; Dong, Z. C., Tip-Enhanced Raman Spectroscopic Imaging of Individual Carbon Nanotubes with Subnanometer Resolution.** ***Nano Lett.*** **2016,** ***16*** **(7), 4040-4046.**
55. **Sheng, S. X.; Wu, J. B.; Cong, X.; Li, W. B.; Gou, J.; Zhong, Q.; Cheng, P.; Tan, P. H.; Chen, L.; Wu, K. H., Vibrational Properties of a Monolayer Silicene Sheet Studied by Tip-Enhanced Raman Spectroscopy.** ***Phys. Rev. Lett.*** **2017,** ***119*** **(19), 196803.**
56. **Kirchhuebel, T.; Gruenewald, M.; Sojka, F.; Kera, S.; Bussolotti, F.; Ueba, T.; Ueno, N.; Rouillé, G.; Forker, R.; Fritz, T., Self-Assembly of Tetraphenyldibenzoperiflanthene (DBP) Films on Ag(111) in the Monolayer Regime.** ***Langmuir*** **2016,** ***32*** **(8), 1981-1987.**
57. **Mehler, A.; Kirchhuebel, T.; Neel, N.; Sojka, F.; Forker, R.; Fritz, T.; Kroger, J., Ordered Superstructures of a Molecular Electron Donor on Au(111).** ***Langmuir*** **2017,** ***33*** **(28), 6978-6984.**
58. **Zhou, Y.; Taima, T.; Kuwabara, T.; Takahashi, K., Efficient Small-Molecule Photovoltaic Cells Using a Crystalline Diindenoperylene Film as a Nanostructured Template.** ***Adv. Mater.*** **2013,** ***25*** **(42), 6069-6075.**
59. **Nakanotani, H.; Higuchi, T.; Furukawa, T.; Masui, K.; Morimoto, K.; Numata, M.; Tanaka, H.; Sagara, Y.; Yasuda, T.; Adachi, C., High-efficiency organic light-emitting diodes with fluorescent emitters.** ***Nat. Commun.*** **2014,** ***5*** **(1), 4016.**
60. **Kiraly, B.; Liu, X.; Wang, L.; Zhang, Z.; Mannix, A. J.; Fisher, B. L.; Yakobson, B. I.; Hersam, M. C.; Guisinger, N. P., Borophene Synthesis on Au(111).** ***ACS Nano*** **2019,** ***13*** **(4), 3816-3822.**
61. **Wu, R.; Drozdov, I. K.; Eltinge, S.; Zahl, P.; Ismail-Beigi, S.; Božović, I.; Gozar, A., Large-area single-crystal sheets of borophene on Cu(111) surfaces.** ***Nat. Nanotechnol.*** **2019,** ***14*** **(1), 44-49.**
62. **Vinogradov, N. A.; Lyalin, A.; Taketsugu, T.; Vinogradov, A. S.; Preobrajenski, A., Single-Phase Borophene on Ir(111): Formation, Structure, and Decoupling from the Support.** ***ACS Nano*** **2019,** ***13*** **(12), 14511-14518.**
63. **Sheng, S. X.; Wu, J. B.; Cong, X.; Zhong, Q.; Li, W. B.; Hu, W. Q.; Gou, J.; Cheng, P.; Tan, P. H.; Chen, L.; Wu, K. H., Raman Spectroscopy of Two-Dimensional Borophene Sheets.** ***ACS Nano*** **2019,** ***13*** **(4), 4133-4139.**
64. **Moskovits, M., Surface selection rules.** ***J. Chem. Phys.*** **1982,** ***77*** **(9), 4408-4416.**
65. **Malard, L. M.; Pimenta, M. A.; Dresselhaus, G.; Dresselhaus, M. S., Raman spectroscopy in graphene.** ***Phys. Rep.*** **2009,** ***473*** **(5), 51-87.**
66. **Zhang, S.; Zhang, N.; Zhao, Y.; Cheng, T.; Li, X.; Feng, R.; Xu, H.; Liu, Z.; Zhang, J.; Tong, L., Spotting the differences in two-dimensional materials - the Raman scattering perspective.** ***Chem. Soc. Rev.*** **2018,** ***47*** **(9), 3217-3240.**
67. **Ferrari, A. C.; Robertson, J., Interpretation of Raman spectra of disordered and amorphous carbon.** ***Phys. Rev. B*** **2000,** ***61*** **(20), 14095-14107.**

68. Huang, M.; Yan, H.; Chen, C.; Song, D.; Heinz, T. F.; Hone, J., Phonon softening and crystallographic orientation of strained graphene studied by Raman spectroscopy. *Proc. Natl. Acad. Sci. U.S.A.* 2009, *106* (18), 7304-7308.
69. Bissett, M. A.; Tsuji, M.; Ago, H., Strain engineering the properties of graphene and other two-dimensional crystals. *Phys. Chem. Chem. Phys.* 2014, *16* (23), 11124-38.
70. Hui, Y. Y.; Liu, X.; Jie, W.; Chan, N. Y.; Hao, J.; Hsu, Y. T.; Li, L. J.; Guo, W.; Lau, S. P., Exceptional tunability of band energy in a compressively strained trilayer MoS2 sheet. *ACS Nano* 2013, *7* (8), 7126-31.
71. Rahaman, M.; Rodriguez, R. D.; Plechinger, G.; Moras, S.; Schuller, C.; Korn, T.; Zahn, D. R. T., Highly Localized Strain in a MoS2/Au Heterostructure Revealed by Tip-Enhanced Raman Spectroscopy. *Nano Lett.* 2017, *17* (10), 6027-6033.
72. Li, Y.; Hu, Z.; Lin, S.; Lai, S. K.; Ji, W.; Lau, S. P., Giant Anisotropic Raman Response of Encapsulated Ultrathin Black Phosphorus by Uniaxial Strain. *Adv. Funct. Mater.* 2017, *27* (19), 1600986.
73. Stroscio, J. A.; Celotta, R. J., Controlling the dynamics of a single atom in lateral atom manipulation. *Science* 2004, *306* (5694), 242-247.
74. Iancu, V.; Deshpande, A.; Hla, S. W., Manipulation of the Kondo effect via two-dimensional molecular assembly. *Phys. Rev. Lett.* 2006, *97* (26), 266603.
75. Perera, U. G. E.; Ample, F.; Kersell, H.; Zhang, Y.; Vives, G.; Echeverria, J.; Grisolia, M.; Rapenne, G.; Joachim, C.; Hla, S. W., Controlled clockwise and anticlockwise rotational switching of a molecular motor. *Nat. Nanotechnol.* 2013, *8* (1), 46-51.
76. Shukla, V.; Grigoriev, A.; Jena, N. K.; Ahuja, R., Strain controlled electronic and transport anisotropies in two-dimensional borophene sheets. *Phys. Chem. Chem. Phys.* 2018, *20* (35), 22952-22960.
77. Amsterdam, S. H.; Marks, T. J.; Hersam, M. C., Leveraging Molecular Properties to Tailor Mixed-Dimensional Heterostructures beyond Energy Level Alignment. *J. Phys. Chem. Lett.* 2021, *12* (19), 4543-4557.
78. Cheng, C.; Sun, J. T.; Liu, H.; Fu, H. X.; Zhang, J.; Chen, X. R.; Meng, S., Suppressed superconductivity in substrate-supported beta(12) borophene by tensile strain and electron doping. *2d Mater* 2017, *4* (2), 025032.

Table of Contents Graphic